Ultracold High-Spin Σ-State Polar Molecules for New Physics Searches

Alessio Ciamei,[1,2,3,*,†] Adam Koza,[4,*] Marcin Gronowski,[4] and Michał Tomza[4,‡]

[1]*Istituto Nazionale di Ricerca Metrologica (INRiM), 50019 Sesto Fiorentino, Italy*
[2]*Istituto Nazionale di Ottica del Consiglio Nazionale delle Ricerche (CNR-INO), 50019 Sesto Fiorentino, Italy*
[3]*European Laboratory for Non-Linear Spectroscopy (LENS), Università di Firenze, 50019 Sesto Fiorentino, Italy*
[4]*Faculty of Physics, University of Warsaw, Pasteura 5, 02-093 Warsaw, Poland*

(Received 23 July 2025; accepted 27 January 2026; published 9 March 2026)

We propose high-spin Σ-state polar molecules assembled from ultracold atoms to probe charge-parity-violating physics beyond the standard model. We identify YbCr as a prime candidate to search for the electric dipole moment of the electron. We show that the combination of relativistic ytterbium and high-spin chromium, amenable to magnetoassociation, leads to molecules with easy-to-polarize parity doublets and large intramolecular electric fields. Based on *ab initio* results for molecular constants, we predict a sensitivity of $\delta d_e = (6 \times 10^{-31}/\sqrt{n_{\mathrm{day}}})\, e\,\mathrm{cm}$ via standard spin-precession measurements, assess the experimental feasibility, and discuss potential extensions to more advanced quantum control as well as searches of the nuclear magnetic quadrupole moment. This work paves the way to next-generation searches for new physics with ultracold molecules in both the leptonic and hadronic sectors.

DOI: 10.1103/wlq7-9p41

Subject Areas: Atomic and Molecular Physics, Particles and Fields, Physical Chemistry

I. INTRODUCTION

Detection of a nonzero electric dipole moment (EDM) of a fundamental particle with today's experimental sensitivities would unequivocally signal charge-parity violation (CPV) beyond the standard model (SM) [1,2] and possibly explain matter-antimatter asymmetry in nature [3–6]. As for the electron EDM (eEDM), atomic-molecular-optics experiments exploit paramagnetic polar molecules, which, thanks to their large internal electric field, offer extreme sensitivity. The most stringent limit $|d_e| < 4.1 \times 10^{-30}\, e\,\mathrm{cm}$ was obtained on trapped HfF^+ ions [7], improving by a factor of 2.5 on the previous bound set by a cryogenic molecular beam of metastable ThO [8]. On the one hand, assuming maximal symmetry violation, these experiments already restrict the mass of conjectured beyond-SM particles leading to CPV above the 4–40 TeV range [7,8], which is well beyond the direct reach of current particle colliders. On the other hand, releasing this assumption but focusing on a certain mass range, they might hint, in combination with particle colliders, to very small CPV phases and the possibility of spontaneous symmetry breaking [9].

While experimental searches have so far used relatively hot molecules, orders of magnitude of improvement in sensitivity is expected by more advanced quantum control at the ultracold temperatures achievable in atomic, molecular, and optical physics experiments [9–11]. Over the past two decades, these platforms have demonstrated exquisite control over neutral atoms, down to the single quantum state and even single-particle control, leading, on the one hand, to quantum simulation and computing and, on the other, to high-precision measurements. More recently, use of optical lattices and tweezers has opened the way to entanglement resources for quantum computing [12–18] and metrology [19–24]. Extension of this experimental toolbox to eEDM-sensitive molecular species would allow dramatic gain in sensitivity even for standard-quantum limit (SQL) spin-precession measurements. High spatial density and low temperature will allow for trapping a large number of molecules, i.e., many repeated measurements, in low-intensity optical traps, i.e., long coherence times without unwanted light shifts. Moreover, those conditions will also allow the application of recently proposed entanglement-enhanced metrology protocols [25]. However, the strategy to get to high phase-space density has remained elusive [10].

Despite tremendous progress to directly laser cool and trap heavy, eEDM-sensitive species, including diatomic

*These authors contributed equally to this work.
†Contact author: ciamei@lens.unifi.it
‡Contact author: michal.tomza@fuw.edu.pl

radicals [26–28] and even polyatomic symmetric top molecules [29,30], the only strategy so far able to deliver molecular gases at high phase-space density relies on the assembly from precooled atoms via magnetic Feshbach resonances (FRs). In this case, colliding atom pairs are associated with a magnetic-field sweep across a FR [31,32] and later transferred to the rovibrational ground state via stimulated Raman adiabatic passage (STIRAP) [33]. This has been experimentally demonstrated on a number of bialkalis (AA) and has led to the creation of molecular quantum gases [34–36] and their application to many-body physics, ultracold chemistry, and quantum computation [15,37–39]. Nonetheless, these species feature a singlet electronic ground state without unpaired electron spins and are, thus, eEDM insensitive. A potential improvement beyond standard AAs, albeit with relatively poor eEDM sensitivities, was identified in alkali-alkaline-earth (AAE) compounds [40]. Despite the experimental discovery of magnetic FRs in these systems [41], their ultranarrow character has so far hindered magnetoassociation. More recently, diatomics isovalent to AAE have been proposed, notably YbAg [42,43] and RaAg [44], which thanks to the high electron affinity of Ag feature a high sensitivity. However, this strategy presents several challenges both for the preparation of the ultracold atomic mixture and for molecule formation due to FRs of similar character as those in AAEs.

In this work, we propose a comprehensive strategy to realize and probe ultracold molecular gases of eEDM sensitive molecules assembled from orbitally isotropic transition-metal chromium ($^7S_3$) and closed-shell ytterbium ($^1S_0$). Thanks to the high electron spin of Cr and the heavy, highly relativistic Yb core, this species meets all experimental requirements, regarding both molecule production and internal structure. While we provide the projected sensitivity for spin-precession experiments within the SQL, extensions to more advanced protocols as well as searches for the nuclear quadrupole magnetic moment are discussed. Finally, this strategy can be applied to other isovalent species, which will further allow probing of hadronic CPV effects.

II. EXPERIMENTAL REQUIREMENTS

How the choice of the molecular species is crucial for eEDM searches is illustrated by considering the quantum-projection noise limited sensitivity valid for SQL spin-precession measurements [45–47]:

$$\delta d_e = \frac{\hbar}{2E_{\mathrm{int}}|\langle\hat{\Sigma}\rangle|\tau\sqrt{N}}. \tag{1}$$

Here, E_{int} is the (state-dependent) internal electric field of the molecule aligned along its internuclear axis $\mathbf{n}$, $|\langle\hat{\Sigma}\rangle| = |\langle\mathbf{S}\cdot\mathbf{n}\rangle|$ is the (state-dependent) projection of the total electron spin $\mathbf{S}$ onto $\mathbf{n}$, τ is the coherent interrogation time, and N is the total number of detected particles. The effective internal electric field is conveniently defined as $E_{\mathrm{eff}} = E_{\mathrm{int}}|\langle\hat{\Sigma}\rangle|$ [47]. Assuming a long τ by virtue of the attainable ultracold temperatures, three main experimental requirements need to be considered: (i) large molecule number N, which implies efficient molecule production; (ii) strong E_{int}, which requires at least one heavy nucleus and one unpaired electron in an s-hybridized orbital; (iii) high $|\langle\hat{\Sigma}\rangle|$ can be easily achieved in species with high electric polarizability featuring parity-doubled states. As we describe later, the existence of such states also allows for robust rejection of systematic errors in the experiment and implementation of more advanced protocols.

III. Ω DOUBLING

The $Yb^{\delta+}Cr^{\delta-}$ bond between Yb ($^1S_0$) and Cr ($^7S_3$) results in a single ground state of the $^7\Sigma^+$ symmetry. The emergence of a Hund's case (a) angular momentum coupling in a Σ state is nontrivial and arises from the presence of strong second-order spin-orbit (and spin-spin) interaction rather than the typical first-order spin-orbit interaction for $\Lambda > 0$ states, with Λ being the electronic orbital angular momentum projection along $\mathbf{n}$. Remarkably, this allows us to obtain Hund's case (a) diatomics from S-term ground-state atoms and, contrarily to a common misconception, endows them with parity doublets. The corresponding Coriolis-mixing-induced splitting decreases rapidly with electron-spin projection $|\Sigma|$ due to the higher perturbation order and makes large $|\Sigma|$ states highly polarizable. Following the literature, we introduce the quantum number $\Omega = \Lambda + \Sigma$, which reduces to $\Omega = \Sigma$ in our case, and refer to such states as Ω-like doublets. The combination of heavy Yb and high-spin Cr ensures the occurrence of this scenario. Introducing the total angular momentum $\mathbf{J}$ excluding nuclear spins, the effective rotational Hamiltonian without external fields can be constructed as follows [48]:

$$\begin{aligned}\mathcal{H}_0 = {} & B_0 T^1(\mathbf{J})\cdot T^1(\mathbf{J}) + (\gamma_0 - 2B_0)T^1(\mathbf{J})\cdot T^1(\mathbf{S}) \\ & + (2\sqrt{6}/3)\lambda_0 T^2_0(\mathbf{S}) + (B_0 - \gamma_0)T^1(\mathbf{S})\cdot T^1(\mathbf{S}),\end{aligned} \tag{2}$$

where the rotational constant $B_0 = 0.041\ \mathrm{cm}^{-1}$, the spin-spin coupling parameter $\lambda_0 = 0.16\ \mathrm{cm}^{-1}$, and the electron spin-rotation coupling constant $\gamma_0 = 9.7\times10^{-4}\ \mathrm{cm}^{-1}$ are calculated with state-of-the-art *ab initio* methods as described in the Appendix and Supplemental Material [49]. Because $\lambda_0/B_0 \gg 1$, the electron spin locks to the internuclear axis with projection Ω and makes ground-state YbCr a good Hund's case (a) molecule for high Ω and low J. Hence, the zero-field eigenstates are labeled in terms of the quantum numbers $|\Omega, J, M_J, e(f)\rangle$, where $e(f)$ denotes ±1 parity according to spectroscopic notation [48]. Useful matrix elements can be found in Supplemental Material [49].

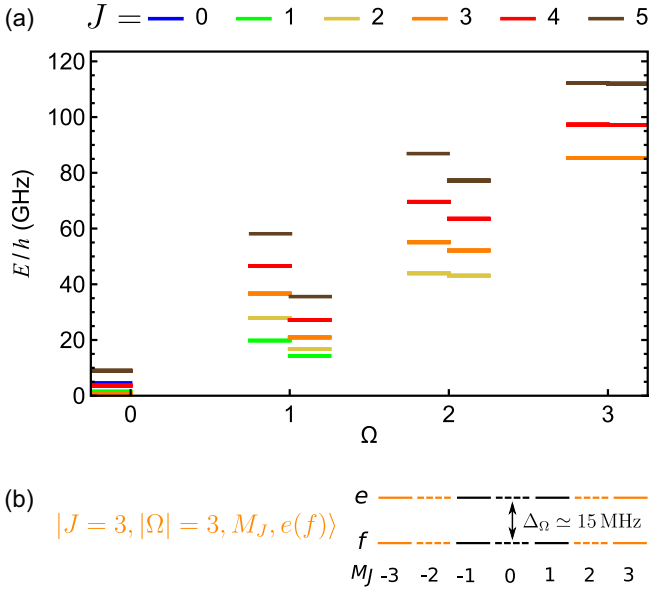

FIG. 1. Rotational spectrum of YbCr molecules. (a) Simulated rotational spectrum for $J \leq 5$ of the ground vibrational level showing the quantization of the electronic spin onto the internuclear axis [Hund's case (a)]. (b) Enlargement of the $J = 3$, $\Omega = 3$ parity doublet.

While appearance of Hund's case (a) rotational spectra in Σ states was understood long ago [72] and Ω doubling was more recently observed in SeO($X^3\Sigma^-$) and CrN($^4\Sigma^-$) [48], the possibility to seize this molecular feature has so far been overlooked in the ultracold molecule community. In passing, we note that to the best of the authors' knowledge no Hund's case (a) $^7\Sigma$ molecule has yet been recorded, as known ground-state diatomics of this symmetry, interesting to astrophysicists, fall into Hund's case (b) (MnH [73] and MnCl [74]). The $^7\Sigma_3^+(J = 3)$ state of YbCr features an Ω doublet with a splitting of about 15 MHz (see Fig. 1 and the Appendix for more details). The effects of external static electric and magnetic fields are easily computed by inclusion of the Stark and Zeeman Hamiltonians in terms of first-rank spherical tensor operators:

$$\mathcal{H}_{\mathrm{St}} + \mathcal{H}_{\mathrm{Z}} = -T^1(\mathbf{D}) \cdot T^1(\mathbf{E}_{\mathrm{lab}}) - g_s \mu_{\mathrm{B}} T^1(\mathbf{S}) \cdot T^1(\mathbf{B}), \quad (3)$$

where the first term describes the interaction of the molecule-frame electric dipole moment $\mathbf{D}$ with the electric field $\mathbf{E}_{\mathrm{lab}}$ and the second term describes the interaction of the electron spin $\mathbf{S}$ with the magnetic field $\mathbf{B}$ through the g factor g_s and Bohr magneton μ_{B} [49]. Here, $\mathbf{D}$ is aligned along $\mathbf{n}$, and its magnitude is 1.24D [49]; the rotational g factor and the electronic magnetic anisotropy of a few 10^{-3} are neglected. In the case of $^7\Sigma_3^+(J = 3)$ states, the polarization $P = |\langle\hat{\Omega}\rangle|/|\Omega|$ as a function of the applied external electric field $E_{\mathrm{lab}} \equiv |\mathbf{E}_{\mathrm{lab}}|$ is shown in Fig. 2. While $P = 0$ for $E_{\mathrm{lab}} = 0$ because $|\Omega, J, M_J, e(f)\rangle$ are parity eigenstates, a modest field of tens of V/cm is sufficient to strongly polarize the molecules in the laboratory frame.

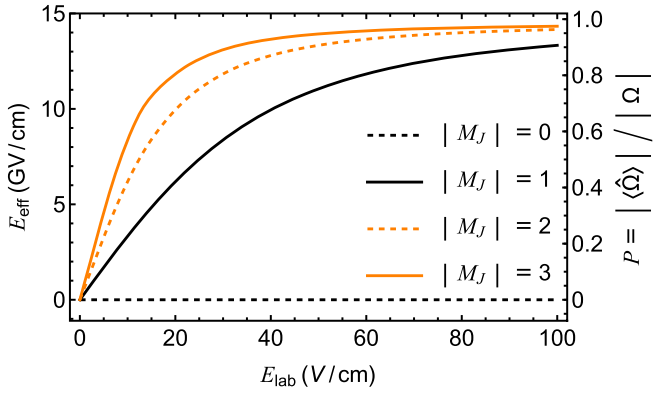

FIG. 2. Effective electric field E_{eff} and polarization P induced by an external static electric field E_{lab} for different $|M_J|$ of $^7\Sigma_3^+(J = 3)$.

IV. eEDM SENSITIVITY

In order to assess the sensitivity of YbCr to the eEDM, we include the effective CPV Hamiltonian:

$$\mathcal{H}_{\mathrm{CPV}} = \mathcal{H}_{\mathrm{SP}} + \mathcal{H}_{\mathrm{eEDM}} = (W_{\mathrm{s}} k_{\mathrm{s}} + W_{\mathrm{d}} d_{\mathrm{e}}) \hat{\Omega}, \quad (4)$$

where $\mathcal{H}_{\mathrm{SP}}$ describes the scalar-pseudoscalar electron-nucleon interaction via the enhancement factor W_{s} and the dimensionless isotope-specific k_{s} parameter and $\mathcal{H}_{\mathrm{eEDM}}$ describes the interaction of the eEDM d_{e} with an effective internal field via the enhancement factor W_{d}. While k_{s} and d_{e} are the focus of the experimental search, W_{s} and W_{d} are computed via *ab initio* methods. The case of YbCr is well described by a single-contributing electron picture, in which the nonbonding s electron orbiting close to the Yb core is the main source of CPV interactions, with $W_{\mathrm{s}} = 4.24\ h\,\mathrm{kHz}$ and $W_{\mathrm{d}} = 1.17 \times 10^{24}\ h\,\mathrm{Hz}/(e\,\mathrm{cm})$ [49]. In the experimental literature, the eEDM Hamiltonian is often expressed in terms of the effective field $\mathcal{H}_{\mathrm{eEDM}} = -\mathbf{d}_e \cdot \mathbf{E}_{\mathrm{eff}}$ with $\mathbf{d}_e = d_e \mathbf{S}/|\langle\hat{\Omega}\rangle|$, $\mathbf{E}_{\mathrm{eff}} = -E_{\mathrm{eff}}\mathbf{n}$, and $E_{\mathrm{eff}} = W_{\mathrm{d}}|\langle\hat{\Omega}\rangle|\mathrm{sgn}(\langle\Omega\rangle) \propto P$, which clearly shows the relation with the polarizability. As shown in Fig. 2, YbCr in $^7\Sigma_3^+(J = 3)$ states offers E_{eff} of about 15 GV/cm at laboratory fields below 100 V/cm. This exceeds by more than one order of magnitude the effective field achievable in AAE compounds [40] and compares well against HfF^+ (approximately 23 GV/cm), which recently set the most stringent limit on the eEDM [7].

V. MOLECULE FORMATION

Bosonic Cr and Yb isotopes are primarily well suited for the proposed application, as they can be efficiently cooled and trapped, and, thanks to their spinless nuclei ($I_{\mathrm{Cr}} = I_{\mathrm{Yb}} = 0$), they are free from hyperfine structure.

Several abundant bosonic isotopes are available for both Yb (^{170,172,174,176}Yb) and Cr (^{50,52,54}Cr), of which ^{174}Yb and ^{52}Cr offer the best performance [50,75,76]. For Yb, the combination of laser lights addressing both the broad $^1S_0 \to {}^1P_1$ and intercombination $^1S_0 \to {}^3P_1$ transitions leads to loading rates in excess of 10^9 atoms/s and tens of μK temperatures [51]. For Cr, the main cooling $^7S_3 \to {}^7P_4$ transition and the additional $^7S_3 \to {}^7P_3$ transition for gray molasses [77], following the all-optical strategy demonstrated in Ref. [52], yield optically trapped samples and loading times similar to the ones of Yb.

Sub-μK temperatures and even simultaneous quantum degeneracy can be readily attained by forced evaporation with no need for sympathetic cooling, between Cr optically pumped into its stretched, high-field seeking state ($m_s = -3$) and spinless Yb. This combination is immune both to dipolar Cr losses and interspecies two-body inelastic collisions. Efficient evaporation will be guaranteed by the similar favorable dynamic polarizabilities ($\alpha_{\mathrm{Cr}} = 89$ a.u. and $\alpha_{\mathrm{Yb}} = 160$ a.u. at 1064 nm) and ideal intraspecies background s-wave scattering lengths of approximately $100a_0$ both for Yb (field-insensitive) and for Cr (narrow and sparse FRs) [78–80]. Detrimental large interspecies scattering, if any, will be cured by zeroing out the s-wave interactions via magnetically tunable FRs. Fast, subsecond evaporation time to quantum degeneracy with final number in excess of 10^5 can be achieved in dynamically shaped traps [81].

According to recent theoretical predictions [53], contrarily to AAE mixtures, the Yb + Cr mixture will exhibit an extremely suitable FR scenario for magnetoassociation, featuring at least one FR immune to two-body inelastic collisions below 250 G with magnetic field widths between 0.1 and 10 G. Moreover, the field-independent (quasi-field-independent) intraspecies scattering of Yb (Cr) in that range [79] will allow to effectively tune the interspecies scattering processes without affecting the intraspecies ones. This scenario is experimentally favorable from different viewpoints: (i) FR widths suitable for association [31], (ii) relatively low magnetic field bias compatible with use of high-permeability magnetic shields [82–85], (iii) easy assignment of FRs, and (iv) ability to efficiently populate sites of 3D optical lattices with heteronuclear doublons by zeroing out interspecies scattering. Magnetoassociation of $\mathrm{Cr}(^7S_3, m_s = -3) + \mathrm{Yb}(^1S_0)$ scattering pairs will result in YbCr molecules in the least-bound vibrational level ($v = -1$) and angular momenta $|N = 2, M_N = -2, S = 3, M_S = -1\rangle$ state, where (N, M_N) and (S, M_S) represent the rotational and spin quantum numbers, respectively [53]. Such weakly bound molecules will be subsequently transferred to the vibrational ground state via STIRAP exploiting optically excited levels supported by either $^7\Sigma^+$ or $^7\Pi$, which correlate to the $\mathrm{Yb}(^3P_1) + \mathrm{Cr}(^7S_3)$ threshold, at convenient laser wavelengths (see the Appendix and Supplemental Material [49]).

VI. PROJECTED SQL SENSITIVITY

The expected sensitivity can be estimated in the case of standard spin-precession measurements developed by eEDM experiments on "hot" molecules featuring Ω doublets in either Hund's case (a) or (c) [7,8,86]. In the case of YbCr, we focus on the $^7\Sigma_3^+(J = 3)$ state and consider the subspace spanned by $|3, 3, M_J = \pm 1, e\rangle$ and $|3, 3, M_J = \pm 1, f\rangle$, which form a top and bottom doublet, respectively; see gray dotted lines in Fig. 3. Under application of a modest external electric field $\mathbf{E}_{\mathrm{lab}}$, states of same M_J but opposite parity get mixed, repelling each other, and are for simplicity denoted $\tilde{e}(\tilde{f})$ correlating to good parity states for vanishing field; see black dotted lines in Fig. 3. As a consequence, the electron spin gets polarized along the internuclear axis, and YbCr gets concurrently polarized in the laboratory frame (cf. Fig. 2). Moreover, the application of an external magnetic field $\mathbf{B}$ induces Zeeman splittings depending only on M_J; see blue dashed lines in Fig. 3. The Stark shift is common mode between the components of each doublet, whereas the differential Zeeman shift is $2g_{e,f}(E)\mu_{\mathrm{B}}B$, with $g_{e,f}(0) \simeq 3/2$ with a relative difference between the doublets below % level for $E_{\mathrm{lab}} \lesssim 100$ V/cm [49]. The energy splittings $\hbar\omega_{e,f} = 2g_{e,f}\mu_{\mathrm{B}}B$ can be probed by Ramsey spectroscopy and, within this approach, offer the maximum sensitivity to eEDM with minimum sensitivity to external field noise among possible $\pm M_J$ pairs in YbCr ground state. Swapping between the "top" and "bottom" doublets enables close-to-ideal *spectroscopic* inversion of the external electric field and yields a phase difference due to the sought-after P, T-odd interaction; see red solid lines in Fig. 3.

Depending on the actual implementation of the STIRAP, one can transfer the YbCr population to $|3, 3, 0, f\rangle$ via

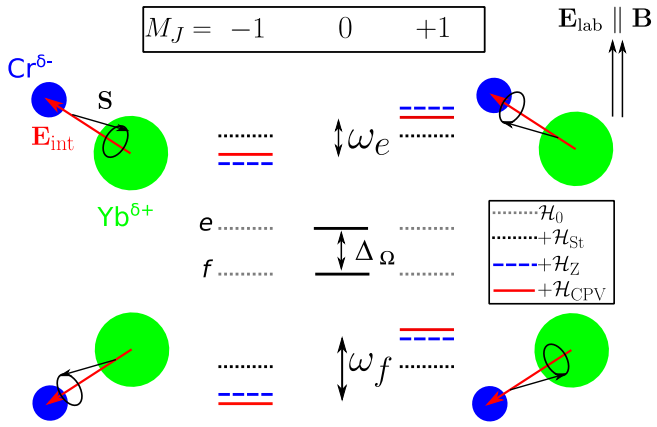

FIG. 3. Energy spectrum of the $M_J = 0, \pm 1$ subspace of $X^7\Sigma_3^+(J = 3)$ due to successive addition of the Stark ($\mathcal{H}_{\mathrm{St}}$), Zeeman ($\mathcal{H}_{\mathrm{Z}}$), and CPV ($\mathcal{H}_{\mathrm{CPV}}$) Hamiltonians to the zero-field $\mathcal{H}_0$. The laboratory electric and magnetic fields are parallel and define the quantization axis. The molecule sketch shows the spatial orientation as well as the electron spin (black arrow) and effective electric field (red arrow).

rapid adiabatic passage and then drive $|3,3,0,f\rangle \rightarrow (|3,3,+1,\tilde{e}\rangle \pm |3,3,-1,\tilde{e}\rangle)/\sqrt{2}$ with a radio-frequency (rf) pulse. The molecular state subsequently evolves freely in a Ramsey scheme accumulating a phase difference ϕ. A second rf pulse will bring a population $\cos^2(\phi)$ back to $|3,3,0,f\rangle$, after which the sensitive part of the measurement is over. Choosing the right time to sit on the maximum slope of the Ramsey fringe will yield the highest phase sensitivity. The leftover population in the doublet will be used for signal normalization. STIRAP, in combination with rf pulses if necessary, will bring YbCr populations back to the least bound vibrational level, encoding the phase information in the Cr spin degree of freedom. Finally, simultaneous dissociation across the almost degenerate FRs for different magnetic sublevels, followed by time of flight under a Stern-Gerlach force and final absorption imaging of Cr, will enable a normalized measurement of the original state populations and extraction of the phase ϕ. In this standard approach, the coherence time will be limited by magnetic-field noise. The stability and homogeneity of the external magnetic field is crucial, as it limits the coherent interrogation time τ. In the case of ultracold YbCr gases, the sample volume of about $(100\ \mu\text{m})^3$ would be much smaller than in previous experiments on "hot" molecules, and use of magnetic-field shielding will help controlling a stable and homogeneous low bias field in the range from 1 to 10 mG which could be further monitored by comagnetometry on unbound Cr atoms. Recent advancements in the field of spinor Bose-Einstein condensates have shown coherence times above 1 s for transitions with μ_B-level sensitivity [82,84]. Using the predicted $E_{\text{eff}} = 14.7$ GV/cm, a coherence time of 1 s, an optimistic but feasible molecule number of 10^5, and 6 s cycle time, we obtain a projected statistical sensitivity of $\delta d_e = (6 \times 10^{-31}/\sqrt{n_{\text{day}}})\ e\,\text{cm}$.

The reported sensitivity appears robust against potential experimental limitations. First, we consider potential systematic effects due to the interaction of the molecules with the trap light used to realize the optical lattices. While the wavelength can be safely chosen to be far detuned from any electric-dipole-allowed transition ($\lambda > 1\ \mu$m) without the need for magic wavelength conditions, the associated vector polarizability mimics the effect of a magnetic field on the Ω doublets, which, if correlated with E reversals, could generate false EDM signals [27,87]. While this effect is ideally canceled by employing lattice beams with perfect linear polarization, it typically results in a stringent requirement on the level of degree of linear polarization. Our strategy, based on ultracold molecules, dramatically relaxes this requirement: Even for subhertz tunneling rates, corresponding to around 100 h kHz absolute well depth originating from the scalar polarizability [54], a suppression of the vector polarizability of 10^{-6} is sufficient to pull this effect below the single-molecule shot noise limit. Considering an order of magnitude suppression due to the ratio between spin-orbit splitting and frequency of the relevant $X^7\Sigma^+ \rightarrow B^7\Sigma^+$ and $X^7\Sigma^+ \rightarrow A^7\Pi$ transitions, this requires the low-power lattice beams to be linearly polarized to better than 10^{-5}, safely larger than the best recorded values [88]. Furthermore, effects of long-range interactions should be addressed since, unlike for quantum metrology protocols, they should be avoided [27]. Here, this is indeed the case even for nearest-neighbor molecules in optical lattice at 1064 nm wavelength (see the Appendix): The differential shift within the doublets, induced by electric dipole-dipole interaction, is zero to first order and $\lesssim 100\ h$ mHz to second order. The differential shift originating from magnetic dipole-dipole is already below this level to first order. Finally, given the small vibrational ($\omega_0 \simeq 90\ \text{cm}^{-1}$), rotational ($B_0 = 0.041\ \text{cm}^{-1}$) [49,54], and spin-spin ($\lambda_0 = 0.16\ \text{cm}^{-1}$) constants [49,53], together with the large energy necessary to address other electronic states via electric-dipole-allowed transitions (approximately $10^4\ \text{cm}^{-1}$), we expect the absorption of blackbody radiation, peaking at about 600 cm^{-1} at room temperature, to be negligible for the proposed experiments, as can be seen comparing with previous results [89].

VII. BEYOND SQL AND HADRONIC CPV

While ground-state YbCr does not provide orbital-spin magnetic moment quasicancellation as in ThO or HfF^+, its internal structure will allow for the engineering of field insensitive transitions [90] and, thanks to the ultracold temperatures, even for the implementation of quantum metrology protocols beyond the standard quantum limit [25]. The latter have been recently proposed for parity-doubled molecules *with* magnetic field sensitivity trapped in optical lattices or optical tweezer arrays.

Moreover, our results can be extended to the search for CP violation in the hadronic sector. The $^{173}\text{Yb}^{52}\text{Cr}$ isotopolog, with its high-spin Yb nucleus ($I = 5/2$), appears an interesting candidate for the search of the nuclear magnetic quadrupole moment (NMQM) with $W_M = 9.48 \times 10^{31}\ h\,\text{Hz}/(e\,\text{cm}^2)$ (see the Appendix), while the nuclear Schiff moment, whose sensitivity is enhanced by octupole deformed nuclei, could be investigated in RaCr [9,91].

VIII. CONCLUSIONS

In summary, we identify high-spin Σ-state polar molecules as ideal molecular species to realize an ultracold molecule platform for eEDM searches. In particular, YbCr satisfies all experimental requirements to potentially gain more than one order of magnitude in sensitivity with already established measurement protocols while allowing for more advanced quantum control. More generally, these results will pave the way to a whole new class of ultracold molecules, like the isovalent Cr/Mo + Yb/Ra or even

Eu/Am-containing diatomics [92], for next-generation CPV searches.

ACKNOWLEDGMENTS

A. C. thanks A. Vutha, N. Hutzler, G. Carugno, G. Santambrogio, and M. Zaccanti for fruitful discussions. We gratefully acknowledge the European Union (ERC, 101042989—QuantMol and 101220504—COMPASS) and the National Science Centre Poland (Grants No. 2020/38/E/ST2/00564 and No. 2024/53/N/ST2/03814) for financial support, Poland's high-performance computing infrastructure PLGrid (HPC Center: ACK Cyfronet AGH) for providing computer facilities and support (computational Grant No. PLG/2024/017527), and the Italian Ministry of University and Research for the Young Researcher Grants No. MSCA_0000042 (PoPaMol) cofunded by the European Union—NextGenerationEU.

DATA AVAILABILITY

The data that support the findings of this article are openly available [93].

APPENDIX

The presented formation and application schemes are based on molecular properties that we predict using state-of-the-art *ab initio* quantum-chemical methods.

1. Ground-state interaction potential and electronic properties

The ground electronic state of the YbCr molecule is described by the $^7\Sigma^+$ molecular term and can be well represented by a single Slater determinant. To calculate the corresponding potential energy curve within the Born-Oppenheimer approximation, we employ the coupled cluster methods with the Hartree-Fock reference. The interaction energy is obtained with the supermolecular approach, including the counterpoise correction, $V_{\rm int}(R) = E_{\rm YbCr}(R) - E_{\rm Yb}(R) - E_{\rm Cr}(R)$, where $E_{\rm YbCr}(R)$ denotes the total energy of the YbCr dimer and $E_{\rm Yb}(R)$ and $E_{\rm Cr}(R)$ are the energies of the atoms computed in the dimer basis [94]. To account for relativistic effects, inner-shell electrons of ytterbium and chromium are replaced by the effective scalar-relativistic pseudopotentials, ECP28MDF [95] and ECP10MDF [96], respectively. The remaining 56 electrons (42 in Yb and 14 in Cr) are correlated and described with the recently developed augmented correlation consistent polarized weighted core-valence quintuple-ζ quality basis sets, aug-cc-pwCV5Z-PP [97].

First, we use the spin-restricted open-shell coupled cluster method with single, double, and noniterative triple excitations, RCCSD(T) [98], in the Molpro program [99,100]. The depth of the potential well with this method is determined to be $D_e = 2775\ \mathrm{cm}^{-1}$ with an equilibrium interatomic separation of $R_e = 6.07a_0$ (in good agreement with the previous values of $2866\ \mathrm{cm}^{-1}$ and $6.05a_0$ [54]). Next, in the composite approach [55], we include the full triple correction within the CCSDT method calculated with the same pseudopotentials and aug-cc-pVTZ-PP basis sets, correlating $6s^2$ and $3d^54s^1$ electrons of ytterbium and chromium, respectively, in the MRCC program [101]. The CCSDT correction makes the original potential well slightly deeper, resulting in the final parameters of $D_e = 3021\ \mathrm{cm}^{-1}$, $R_e = 6.05a_0$, $\omega_e = 90.2\ \mathrm{cm}^{-1}$, and $B_e = 0.041\ \mathrm{cm}^{-1}$ for ^{174}Yb^{52}Cr. The obtained potential energy curve is presented in Fig. 4.

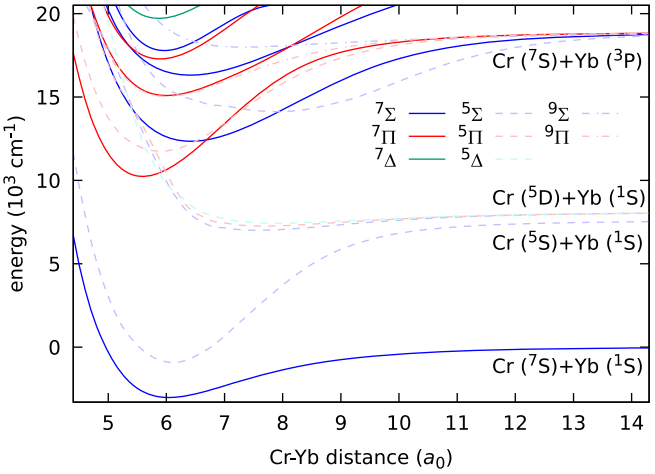

FIG. 4. Potential energy curves of the ground and excited electronic states of the YbCr molecule.

We also calculate the molecule-frame electric dipole moment using the finite-field method. At the CCSD(T) level of theory, the dipole moment at the equilibrium geometry is found to be 1.14D in agreement with the previous value of 1.19D [54]. Inclusion of a correction for full triple excitations increases this value to 1.24D.

2. Excited electronic states

Successful formation and further precision measurements with YbCr molecules require the efficient transfer of the weakly bound Feshbach dimers to the ground vibrational level via STIRAP. We calculate several electronically excited states of the YbCr molecule to guide this process. Because of the presence of an open d shell in chromium and a p shell in the excited state of ytterbium, one has to deal with a rich manifold of molecular electronic configurations. We consider three families of electronic states that arise from different asymptotic atomic configurations. The first family corresponds to $\mathrm{Cr}(^7\mathrm{S}) + \mathrm{Yb}(^1\mathrm{S})$, leading to the already-calculated ground $^7\Sigma^+$ molecular state. The second involves $\mathrm{Cr}(^5\mathrm{D}) + \mathrm{Yb}(^1\mathrm{S})$, resulting in the $^5\Sigma^+$, $^5\Pi$, and $^5\Delta$ states. The third family originates from

$Cr(^7S) + Yb(^3P)$ and gives rise to the $^5\Sigma^+$, $^5\Pi$, $^7\Sigma^+$, $^7\Pi$, $^9\Sigma^+$, and $^9\Pi$ states.

We calculate the septet states using the equation-of-motion coupled cluster method with single and double excitations (EOM-CCSD) [102] and the nonet states with the regular CCSD method, while the quintet states are obtained with the multireference configuration interaction method with single and double excitations (MRCISD) [103] due to numerical difficulties with EOM-CCSD for low-spin states. The same effective core potentials as for the ground state and the aug-cc-pwCVTZ-PP basis sets [97] are used. EOM-CCSD calculations employed CFOUR [104,105], and MRCI calculations employed Molpro. The final potential energy curves are shown in Fig. 4.

The STIRAP scheme, using the excited $A^7\Pi$ or $B^7\Sigma^+$ state to support an intermediate level, appears to be the most promising. Following Ref. [56], we predict favorable Franck-Condon factors ($\gtrsim 10^{-4}$) for pump and Stokes transitions to vibrational levels of the $A^7\Pi_4$ state around 7000 cm^{-1} below the intercombination line of Yb, but detailed studies of STIRAP are beyond the scope of this work. In the future, the spin-orbit coupling and other electronic states should be included to obtain a more complete prediction.

3. eEDM sensitivity

Heavy, paramagnetic diatomic molecules composed of zero-nuclear-spin isotopes provide an ideal test bed for probing P, T-odd interactions in the (semi)leptonic sector. The dominant sources of CP-violating energy shifts in molecular spectra are the eEDM and the scalar-pseudoscalar electron-nucleon coupling (eN-SPS). Here, we focus on determining the molecular enhancement factors present in Eq. (4). Accurate theoretical modeling is indispensable, because these factors cannot be determined experimentally. To this end, we first solve the many-electron problem with the Dirac-Coulomb Hamiltonian with exact treatment of two-electron integrals over the small components of the wave function using the DIRAC24 package [106]. We generate molecular spinors using the average of configurations Dirac-Coulomb-Hartree-Fock (DCHF) method with six electrons distributed over six Kramers pairs (12 spinors), yielding open-shell spinors composed of ytterbium $6s$ and chromium $3d4s$ orbitals. Building on this DCHF reference, we then perform the multireference configuration interaction (MRCI) calculation using the Kramers-restricted configuration interaction (KRCI) module with the generalized active space (GAS) formalism to capture the electron correlation [107]. MRCI with single and double excitations (MRCISD) and with single, double, and triple excitations (MRCISD) is used with different GASs. All computations employ the uncontracted Dyall basis sets [57]. Finally, we evaluate the expectation value of the eEDM Hamiltonian [108] with respect to the electronic wave function $|\Psi_{^7\Sigma_\Omega}\rangle$, which is given by

$$W_{\mathrm{d}} = \frac{2ic}{\Omega}\left\langle \Psi_{^7\Sigma_\Omega}\left|\sum_j^{N_{\mathrm{e}}} \gamma_j^0\gamma_j^5 p_j^2\right|\Psi_{^7\Sigma_\Omega}\right\rangle, \tag{A1}$$

where i is an imaginary unit, c is the speed of light, γ_j^k are the Dirac matrices, p_j is the linear momentum operator of electron, and N_{e} is the number of electrons. Similarly, for the eN-SPS enhancement factor [109], we have the following expression:

$$W_{\mathrm{s}} = \frac{iG_{\mathrm{F}}Z}{\sqrt{2}\Omega}\left\langle \Psi_{^7\Sigma_\Omega}\left|\sum_j^{N_{\mathrm{e}}} \gamma_j^0\gamma_j^5\rho(r_j)\right|\Psi_{^7\Sigma_\Omega}\right\rangle, \tag{A2}$$

where G_{F} is the Fermi coupling constant, Z is the atomic number, $\rho(r_j)$ is the nuclear charge distribution, and r_j is the position of the jth electron with respect to the nucleus. We compute both enhancement factors for the equilibrium geometry taken from our scalar-relativistic calculations ($R_e = 6.05a_0$). The final value of the eEDM factor is $W_{\mathrm{d}} = 1.17 \times 10^{24}\ h\,\mathrm{Hz}/(e\,\mathrm{cm})$, and the eN-SPS factor is $W_s = 4.24\ h\,\mathrm{kHz}$. Detailed analysis of the convergence of those values concerning the number of correlated electrons, the size of active space, and the basis set cardinality is presented in Supplemental Material [49].

4. Hadronic *CP* violation

The YbCr molecule can also be an interesting candidate for studying CP violation in the hadronic sector. Here, symmetry-violating effects can arise from P, T-odd electromagnetic moments in nuclei. One is the nuclear magnetic quadrupole moment, which has a nonzero value for systems with a nuclear spin $I > 1/2$. The NMQM couples to the magnetic field gradient produced by unpaired electrons, leading to the experimentally observable shifts in spectra. The sensitivity of potential experiments can be significantly enhanced by using molecules containing deformed nuclei due to the collective effects [110]. Notably, among stable ytterbium isotopes, ^{173}Yb (with $I = 5/2$) exhibits significant deformation, making ^{173}YbCr a potentially attractive candidate for molecular NMQM searches. Theoretically, the NMQM can be modeled by the following Hamiltonian [111]:

$$\mathcal{H}_{\mathrm{NQMM}} = -\frac{M}{2I(2I-1)}T_{jk}\sum_i^{N_{\mathrm{e}}}\frac{3}{2}\frac{[\boldsymbol{\alpha}_i\times\mathbf{r}_i]_j}{r_i^5}[r_i]_k, \tag{A3}$$

where M is the NMQM, T_{jk} are the components of the second-rank tensor $T_{jk} = I_jI_k + I_kI_j - \frac{2}{3}I(I+1)\delta_{jk}$ with I the nuclear spin, $\boldsymbol{\alpha}_i$ are the Dirac matrices, and $\mathbf{r}$ is the

position of an electron with respect to the nucleus. For diatomic molecules, this Hamiltonian can be simplified and written in the following way:

$$\mathcal{H}_{\text{eff-NQMM}} = -\frac{MW_{\text{M}}}{2I(2I-1)}\mathbf{J}_e \cdot T \cdot \hat{\mathbf{n}}, \tag{A4}$$

where $\mathbf{J}_e$, I, and $\hat{\mathbf{n}}$ are the total electronic angular momentum, the nuclear spin, and the unit vector along the internuclear axis, respectively. W_{M} is the molecular enhancement factor that needs to be calculated theoretically. In the present work, we evaluate the following matrix element to obtain a numerical value of W_{M} for Yb in the YbCr molecule:

$$W_{\text{M}} = \frac{3}{2\Omega}\left\langle \Psi_{^7\Sigma_\Omega} \middle| \sum_i^{N_e} \left(\frac{\boldsymbol{\alpha}_i \times \mathbf{r}_i}{r_i^5}\right)_z r_z \middle| \Psi_{^7\Sigma_\Omega} \right\rangle, \tag{A5}$$

where Ω is the projection of the total electronic angular momentum $\mathbf{J}_e$ on the molecular axis and z means projection on the molecular axis. The final value of the NQMM factor is $W_{\text{M}} = 9.48 \times 10^{31}\ h\,\text{Hz}/(e\,\text{cm}^2)$. Detailed analysis of the convergence of this value concerning the number of correlated electrons, the size of active space, and the basis set cardinality is presented in Supplemental Material [49].

5. Zero-field splitting

For molecules with at least two unpaired electrons ($S \geq 1$), even in a Σ state with no first-order spin-orbit coupling, the degeneracy of magnetic sublevels is lifted by the spin-spin interaction, leading to the so-called zero-field splitting. This interaction can be described by the tensor that reduces to a single component D for Σ-state diatomic molecules and is connected to the spin-spin coupling parameter λ in Eq. (2) via $D = 2\lambda$. The corresponding effective molecule-frame Hamiltonian is

$$\mathcal{H}_{\text{SS}} = D(\hat{\Sigma}^2 - \mathbf{S}^2/3). \tag{A6}$$

There are two contributions to this interaction: the direct spin-spin magnetic dipolar coupling between open-shell electrons and the spin-orbit coupling in the second order of perturbation theory.

We calculate the zero-field splitting parameter D using wave-function-based methods and density functional theory (DFT). We find that the magnetic dipolar spin-spin contribution within the DFT methodology is not significantly affected by the choice of the functional and is on the order of 0.009 cm^{-1}. It is obtained as an expectation value with the uncontracted all-electron x2c-QZVPPall basis sets [58] and scalar relativistic effects treated at the spin-free two-component formalism (X2C) [112] in the ORCA program [113,114]. In contrast, the second-order spin-orbit contribution, which dominates the total D value (over 95%), is highly sensitive to variations in the used exchange-correlation functional, basis set, and formalism applied in the calculations; thus, it should be treated with care. Because calculations as the sum over states do not provide sufficient accuracy, we extract the second-order spin-orbit contribution by fitting the splitting $D[\Omega^2 - S(S+1)/3]$, resulting from Eq. (A6), to potential energies obtained from solving the many-electron Dirac-Coulomb Hamiltonian for different $^7\Sigma_\Omega$ states with the same methods and basis sets as for the eEDM sensitivity factors. Following extensive computational analyses based on the KRCI method, variations in basis set size, different reference spinors, and correlation treatment, we find the zero-field splitting parameter of $D = 0.32(10)\ \text{cm}^{-1}$, in good agreement with a DFT value reported in Ref. [53]. A comprehensive numerical assessment and experimental implications are provided in Supplemental Material [49].

6. Hund's case transition in YbCr

The ratio λ/B between the spin-spin coupling parameter λ and the rotational constant B, appearing in the effective Hamiltonian of Eq. (2), is crucial, as it dictates the angular momentum coupling scheme for diatomics in $^{2S+1}\Sigma$ electronic states with $S > 1/2$. The transition from Hund's case (a) to case (b) in terms of λ/B is well known, and it is an instructive exercise to look at Cr-bearing high-spin diatomics. For $\lambda/B \gg 1$, e.g., ground-state $X^4\Sigma^-$ CrN, the electron spin locks to the internuclear axis with projection Ω and leads to Hund's case (a) molecule for high $\Omega > 1$ and low total angular momentum J (we follow the literature in using the quantum number $\Omega = \Sigma$ with $\Lambda = 0$). Hence, the zero-field eigenstates are labeled in terms of the quantum numbers $|\Omega, J, M_J, e(f)\rangle$, where $e(f)$ denotes ± 1 parity according to spectroscopic notation. For $\lambda/B < 1$ instead, e.g., ground-state $X^6\Sigma^+$ CrH, the electronic spin is mostly decoupled from the internuclear axis, leading to a perturbative splitting of the underlying rotational series, with good basis $|J, N, M_J\rangle$. Generally speaking, heavy constituents tend to lead to lower B and, concurrently, to larger λ, dominated by second-order spin-orbit coupling rather than direct spin-spin interaction for elements beyond the first row of the periodic table. Hence, heavier species more often approximate Hund's case (a), compared to lighter species, which usually fall into case (b).

However, in a diatomic molecule, λ and B also depend on the vibrational level of interest for which the effective Hamiltonian is employed. Thus, in principle, a transition between cases (a) and (b) is possible and indeed occurs for YbCr. This is mostly due to the different scaling of these two quantities, with λ typically featuring a double exponential decay with the internuclear distance r and B a simple power law $\propto r^{-2}$, which suggests that Hund's case (a) is privileged in the vibrational ground state while case (b) in excited levels. In order to show this point, we exploit the *ab initio* λ [53] and the potential energy

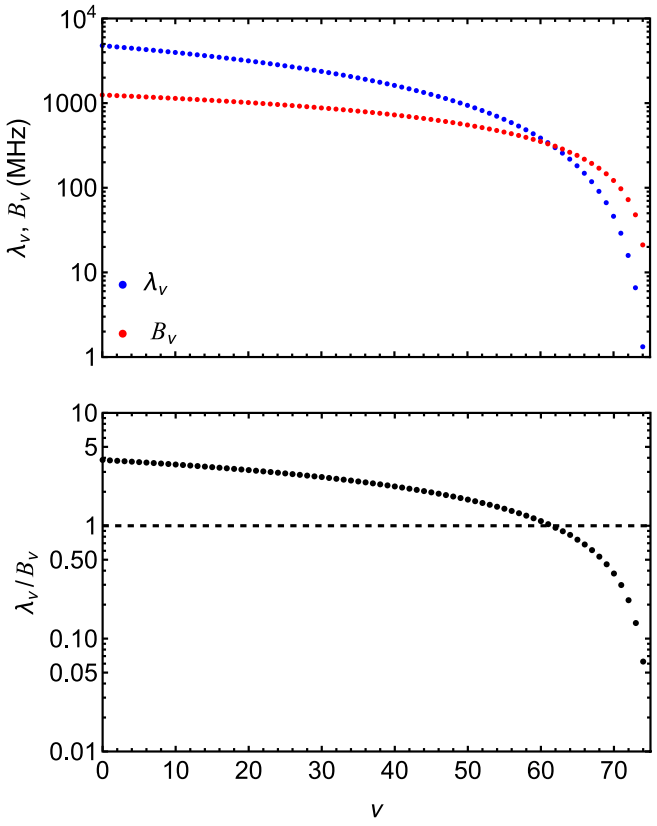

FIG. 5. Hund's case transition in YbCr. Top: spin-spin coupling parameter (blue curve) and rotational constant (red curve) as a function of the vibrational quantum number v. Bottom: ratio between them as function of the vibrational quantum number v. Values much higher than unity (dashed line) tend to case (a), while points much lower than that tend to case (b).

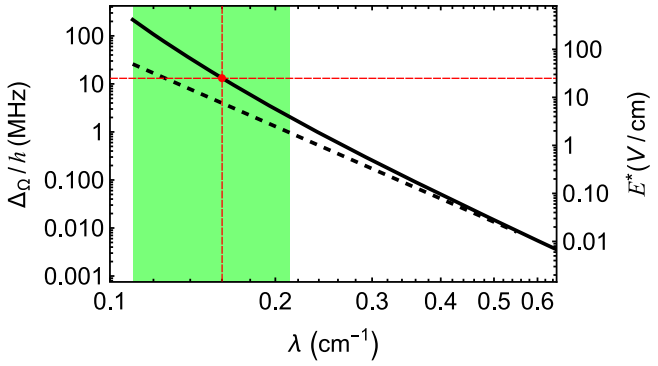

FIG. 6. Effect of the variation of the spin-spin parameter λ_0 on the Ω-doublet splitting Δ_Ω and polarizing field E^* for $J = |\Omega| = 3$. The green shaded area marks the confidence region predicted by our *ab initio* methods, and the red circle is the mean expected value $\lambda_0 = 0.16$ cm^{-1}. The solid black curves is the numerical simulation, while the black dashed line shows the asymptotic trend, well captured by perturbation theory fitted to large-λ numerics.

curve [54] to extract B; see also additional, consistent *ab initio* results above. The irreducible tensor representation $2\lambda(r)T^2(\mathbf{S},\mathbf{S})\cdot T^2(\mathbf{n},\mathbf{n})$ used in Ref. [53], of which we consider the diagonal $q = 0$ component, is identical to our effective Hamiltonian, with the same numerical value of λ_0, knowing that the average $\langle T_0^2(\mathbf{n},\mathbf{n})\rangle = 2/\sqrt{6}$ [48]. We introduce the notation $\lambda_v = \langle v|\lambda(r)|v\rangle$ and $B_v = \langle v|1/(2\mu r^2)|v\rangle$ to make the dependence on the vibrational degree of freedom explicit. Figure 5 shows λ_v and B_v (top), as well as their ratio (bottom) for the ground-state YbCr as a function of the vibrational quantum number. As explained in the main text, Hund's case (a) becomes a good approximation towards the vibrational ground state, especially for high Ω and low J.

To which extent YbCr is a pure Hund's case (a) molecule in its vibrational ground state is determined by λ_0/B_0. In particular, the splitting between parity doublets Δ_Ω originates from Coriolis mixing as a $2|\Omega|$th-order effect in perturbation theory leading to $\Delta_\Omega/\lambda_0 \propto (B_0/\lambda_0)^{2|\Omega|}$. While B_0 is predicted with a % -level relative uncertainty by *ab initio* calculations, the calculation of λ_0 is challenging, since it involves contributions from electronically excited states; see above and Supplemental Material [49]. That is why the main uncertainty on the rotational spectrum of YbCr stems from $\lambda_0 = 0.16(5)$ cm^{-1}. Within this range, and focusing on the relevant for $J = |\Omega| = 3$ states, the proposed experiment, protocols, and projected sensitivity are valid. In Fig. 6, we show the effect of the variation of λ_0 within our confidence region on the Δ_Ω ($\Omega = 3$) and on the required electric field E^* for 50% polarization, i.e., $P = |\langle\hat{\Omega}\rangle|/3 = 0.5$. Useful matrix elements can be found in Supplemental Material [49].

7. Dipolar interactions

Effects of intermolecular interactions should be addressed since, unlike for quantum metrology protocols, they should be avoided in standard spin-precession experiments [27]. In this case, we are sensitive to differential shifts within top ($|3,3,\pm1,\tilde{e}\rangle$) and bottom ($|3,3,\pm1,\tilde{f}\rangle$) doublets, induced by either electric or magnetic interactions. The interaction energy between electric (E) and magnetic (M) dipoles reads

$$V^{\mathrm{dd}}_{\mathrm{E(M)}} = \alpha_{\mathrm{E(M)}}\frac{\boldsymbol{\mu}^1\cdot\boldsymbol{\mu}^2 - 3(\boldsymbol{\mu}^1\cdot\hat{R})(\boldsymbol{\mu}^2\cdot\hat{R})}{R^3}, \qquad \text{(A7)}$$

where the electric or magnetic dipoles $\boldsymbol{\mu}^{1(2)} = \boldsymbol{\mu}^{1(2)}_{\mathrm{E(M)}}$ are separated by the cartesian vector $\mathbf{R} = R\hat{R}$ and the constants are either $\alpha_E = (4\pi\epsilon_0)^{-1}$ or $\alpha_M = (4\pi)^{-1}\mu_0$, where ϵ_0 is the vacuum permittivity and μ_0 is the vacuum magnetic permeability. Reverting to the irreducible spherical tensor representation in the laboratory frame, we obtain the following expressions for the dipolar Hamiltonian [48]:

$$\mathcal{H}^{\mathrm{dd}}_{\mathrm{E(M)}} = -\alpha_{\mathrm{E(M)}}\sqrt{6}T^2(\boldsymbol{\mu}_1,\boldsymbol{\mu}_2)\cdot T^2(C), \qquad \text{(A8)}$$

where $T^2(\boldsymbol{\mu}_1, \boldsymbol{\mu}_2)$ is the second-rank tensor composed of first-rank tensors $T^1_p(\boldsymbol{\mu}_{1(2)})$ and $T^2(C)$ denotes second-rank reduced spherical harmonics. The laboratory-frame $T^1_p(\boldsymbol{\mu}_{1(2)})$ are conveniently expressed in terms of molecule-frame matrix elements:

$$T^1_p(\boldsymbol{\mu}) = \sum_q \mathcal{D}^1_{p,q}(w)^* T^1_q(\boldsymbol{\mu}), \tag{A9}$$

with $\mathcal{D}^1_{p,q}(w)^*$ being the complex conjugate of the p, q element of the first-rank Wigner $\mathcal{D}$ rotation matrix.

We first consider the electric dipolar interaction between a pair of YbCr molecules:

$$\mathcal{H}^{\mathrm{dd}}_{\mathrm{E}} = -\alpha_{\mathrm{E}}\sqrt{6}T^2(\mathbf{D_1}, \mathbf{D_2}) \cdot T^2(C), \tag{A10}$$

with molecule-frame matrix elements $\langle\Sigma'|T^1_0(\mathbf{D})|\Sigma\rangle = \delta_{\Sigma,\Sigma'}D$ and $T^1_{\pm1}(\mathbf{D}) = 0$. To first order, the differential shift within a doublet $\tilde{e}$ or $\tilde{f}$ can be evaluated considering the molecule-pair states $\{|M_1, M_2\rangle\}$, where $M_i = \pm 1$ refer to single molecule states. Diagonal matrix elements of $\mathcal{H}^{\mathrm{dd}}_{\mathrm{E}}$ are identical; hence, the differential shift within a doublet is zero to lowest order. This result is expected, since the laboratory-frame orientation of the molecules within a doublet is identical and the expectation value of $\mathcal{H}^{\mathrm{dd}}_{\mathrm{E}}$ is simply the dipole-dipole interaction of two vertically aligned dipoles $\boldsymbol{\mu}^{1(2)}_{\mathrm{E}} = PD|\Omega|[J(J+1)]^{-1}\hat{z}$, where P is the degree of polarization. To second order, we need instead to consider coupling to virtual states outside the basis spanned by the spin-precession doublets. We find that the dominant contributions come from within the subspace of the same "parity" $\tilde{e}$ (or $\tilde{f}$), e.g., $|+1,-1\rangle \leftrightarrow |0,0\rangle$ and $|+1,-1\rangle \leftrightarrow |\pm 2,0\rangle$, which are smaller than or comparable to single-molecule shot noise ($\lesssim$100 h mHz) even for nearest-neighbor molecules in a 3D optical lattice with $\lambda = 1064$ nm.

We now move to the magnetic dipolar interaction dominated by the electron spins:

$$\mathcal{H}^{\mathrm{dd}}_{\mathrm{M}} = -\alpha_{\mathrm{M}} g_s^2 \mu_{\mathrm{B}}^2 \sqrt{6} T^2(\mathbf{S_1}, \mathbf{S_2}) \cdot T^2(C), \tag{A11}$$

with the relevant molecule-frame matrix elements being

$$\langle\Sigma|T^1_q(\mathbf{S})|\Sigma'\rangle = (-1)^{S-\Sigma}\begin{pmatrix} S & 1 & S \\ -\Sigma & q & \Sigma' \end{pmatrix}\sqrt{S(S+1)(2S+1)}. \tag{A12}$$

The differential shift originating from magnetic dipole-dipole is already well below the single-molecule shot noise to first order even for nearest-neighbor molecules in the same optical lattice.

[1] M. S. Safronova, D. Budker, D. DeMille, D. F. J. Kimball, A. Derevianko, and C. W. Clark, *Search for new physics with atoms and molecules*, Rev. Mod. Phys. **90**, 025008 (2018).

[2] T. E. Chupp, P. Fierlinger, M. J. Ramsey-Musolf, and J. T. Singh, *Electric dipole moments of atoms, molecules, nuclei, and particles*, Rev. Mod. Phys. **91**, 015001 (2019).

[3] M. Dine and A. Kusenko, *Origin of the matter-antimatter asymmetry*, Rev. Mod. Phys. **76**, 1 (2004).

[4] L. Canetti, M. Drewes, and M. Shaposhnikov, *Matter and antimatter in the universe*, New J. Phys. **14**, 095012 (2012).

[5] A. D. Sakharov, *Violation of CP invariance, C asymmetry, and baryon asymmetry of the universe*, Pis'ma Zh. Eksp. Teor. Fiz. **32**, 392 (1967).

[6] C. Patrignani, *Review of Particle Physics*, Chin. Phys. C **40**, 100001 (2016).

[7] T. S. Roussy, L. Caldwell, T. Wright, W. B. Cairncross, Y. Shagam, K. B. Ng, N. Schlossberger, S. Y. Park, A. Wang, J. Ye, and E. A. Cornell, *An improved bound on the electron's electric dipole moment*, Science **381**, 46 (2023).

[8] V. Andreev, D. G. Ang, D. DeMille, J. M. Doyle, G. Gabrielse, J. Haefner, N. R. Hutzler, Z. Lasner, C. Meisenhelder, B. R. O'Leary, C. D. Panda, A. D. West, E. P. West, and X. Wu (ACME Collaboration), *Improved limit on the electric dipole moment of the electron*, Nature (London) **562**, 355 (2018).

[9] R. Alarcon, J. Alexander, V. Anastassopoulos *et al.*, *Electric dipole moments and the search for new physics*, arXiv:2203.08103.

[10] D. DeMille, N. R. Hutzler, A. M. Rey, and T. Zelevinsky, *Quantum sensing and metrology for fundamental physics with molecules*, Nat. Phys. **20**, 741 (2024).

[11] J. Ye and P. Zoller, *Essay: Quantum sensing with atomic, molecular, and optical platforms for fundamental physics*, Phys. Rev. Lett. **132**, 190001 (2024).

[12] M. Saffman, *Quantum computing with atomic qubits and Rydberg interactions: Progress and challenges*, J. Phys. B **49**, 202001 (2016).

[13] L. Henriet, L. Beguin, A. Signoles, T. Lahaye, A. Browaeys, G.-O. Reymond, and C. Jurczak, *Quantum computing with neutral atoms*, Quantum **4**, 327 (2020).

[14] A. Browaeys and T. Lahaye, *Many-body physics with individually controlled Rydberg atoms*, Nat. Phys. **16**, 132 (2020).

[15] A. M. Kaufman and K.-K. Ni, *Quantum science with optical tweezer arrays of ultracold atoms and molecules*, Nat. Phys. **17**, 1324 (2021).

[16] A. J. Daley, I. Bloch, C. Kokail, S. Flannigan, N. Pearson, M. Troyer, and P. Zoller, *Practical quantum advantage in quantum simulation*, Nature (London) **607**, 667 (2022).

[17] D. González-Cuadra, D. Bluvstein, M. Kalinowski, R. Kaubruegger, N. Maskara, P. Naldesi, T. V. Zache, A. M. Kaufman, M. D. Lukin, H. Pichler, B. Vermersch, J. Ye, and P. Zoller, *Fermionic quantum processing with programmable neutral atom arrays*, Proc. Natl. Acad. Sci. U.S.A. **120**, e2304294120 (2023).

[18] T. Kusano, Y. Nakamura, R. Yokoyama, N. Ozawa, K. Shibata, T. Takano, Y. Takasu, and Y. Takahashi,

Plane-selective manipulations of nuclear spin qubits in a three-dimensional optical tweezer array, Phys. Rev. Res. **7**, L022045 (2025).

[19] A. Ludlow, *"Tweezer clock" offers new possibilities in timekeeping*, Physics **12** (2019).

[20] L. Pezzè, A. Smerzi, M. K. Oberthaler, R. Schmied, and P. Treutlein, *Quantum metrology with nonclassical states of atomic ensembles*, Rev. Mod. Phys. **90**, 035005 (2018).

[21] B. K. Malia, Y. Wu, J. Martínez-Rincón, and M. A. Kasevich, *Distributed quantum sensing with mode-entangled spin-squeezed atomic states*, Nature (London) **612**, 661 (2022).

[22] G. Bornet, G. Emperauger, C. Chen, B. Ye, M. Block, M. Bintz, J. A. Boyd, D. Barredo, T. Comparin, F. Mezzacapo, T. Roscilde, T. Lahaye, N. Y. Yao, and A. Browaeys, *Scalable spin squeezing in a dipolar Rydberg atom array*, Nature (London) **621**, 728 (2023).

[23] W. J. Eckner, N. Darkwah Oppong, A. Cao, A. W. Young, W. R. Milner, J. M. Robinson, J. Ye, and A. M. Kaufman, *Realizing spin squeezing with Rydberg interactions in an optical clock*, Nature (London) **621**, 734 (2023).

[24] J. M. Robinson, M. Miklos, Y. M. Tso, C. J. Kennedy, T. Bothwell, D. Kedar, J. K. Thompson, and J. Ye, *Direct comparison of two spin-squeezed optical clock ensembles at the* 10^{-17} *level*, Nat. Phys. **20**, 208 (2024).

[25] C. Zhang, P. Yu, A. Jadbabaie, and N. R. Hutzler, *Quantum-enhanced metrology for molecular symmetry violation using decoherence-free subspaces*, Phys. Rev. Lett. **131**, 193602 (2023).

[26] J. Lim, J. R. Almond, M. A. Trigatzis, J. A. Devlin, N. J. Fitch, B. E. Sauer, M. R. Tarbutt, and E. A. Hinds, *Laser cooled* YbF *molecules for measuring the electron's electric dipole moment*, Phys. Rev. Lett. **120**, 123201 (2018).

[27] N. J. Fitch, J. Lim, E. A. Hinds, B. E. Sauer, and M. R. Tarbutt, *Methods for measuring the electron's electric dipole moment using ultracold* YbF *molecules*, Quantum Sci. Technol. **6**, 014006 (2020).

[28] F. Kogel, M. Rockenhäuser, R. Albrecht, and T. Langen, *A laser cooling scheme for precision measurements using fermionic barium monofluoride* ($^{137}Ba^{19}F$) *molecules*, New J. Phys. **23**, 095003 (2021).

[29] L. Anderegg, N. B. Vilas, C. Hallas, P. Robichaud, A. Jadbabaie, J. M. Doyle, and N. R. Hutzler, *Quantum control of trapped polyatomic molecules for eEDM searches*, Science **382**, 665 (2023).

[30] Y. Chamorro, A. Borschevsky, E. Eliav, N. R. Hutzler, S. Hoekstra, and L. c. v. F. Pašteka, *Molecular enhancement factors for the* $\mathcal{P}, \mathcal{T}$*-violating electric dipole moment of the electron in* $BaCH_3$ *and* $YbCH_3$ *symmetric top molecules*, Phys. Rev. A **106**, 052811 (2022).

[31] T. Köhler, K. Góral, and P. S. Julienne, *Production of cold molecules via magnetically tunable Feshbach resonances*, Rev. Mod. Phys. **78**, 1311 (2006).

[32] C. Chin, R. Grimm, P. Julienne, and E. Tiesinga, *Feshbach resonances in ultracold gases*, Rev. Mod. Phys. **82**, 1225 (2010).

[33] N. V. Vitanov, A. A. Rangelov, B. W. Shore, and K. Bergmann, *Stimulated raman adiabatic passage in physics, chemistry, and beyond*, Rev. Mod. Phys. **89**, 015006 (2017).

[34] G. Valtolina, K. Matsuda, W. G. Tobias, J.-R. Li, L. De Marco, and J. Ye, *Dipolar evaporation of reactive molecules to below the Fermi temperature*, Nature (London) **588**, 239 (2020).

[35] M. Duda, X.-Y. Chen, A. Schindewolf, R. Bause, J. von Milczewski, R. Schmidt, I. Bloch, and X.-Y. Luo, *Transition from a polaronic condensate to a degenerate Fermi gas of heteronuclear molecules*, Nat. Phys. **19**, 720 (2023).

[36] N. Bigagli, W. Yuan, S. Zhang, B. Bulatovic, T. Karman, I. Stevenson, and S. Will, *Observation of Bose–Einstein condensation of dipolar molecules*, Nature (London) **631**, 289 (2024).

[37] T. Karman, M. Tomza, and J. Pérez-Ríos, *Ultracold chemistry as a testbed for few-body physics*, Nat. Phys. **20**, 722 (2024).

[38] S. L. Cornish, M. R. Tarbutt, and K. R. A. Hazzard, *Quantum computation and quantum simulation with ultracold molecules*, Nat. Phys. **20**, 730 (2024).

[39] C. M. Holland, L. Yukai, and L. W. Cheuk, *On-demand entanglement of molecules in a reconfigurable optical tweezer array*, Science **382**, 1143 (2023).

[40] E. R. Meyer and J. L. Bohn, *Electron electric-dipole-moment searches based on alkali-metal- or alkaline-earth-metal-bearing molecules*, Phys. Rev. A **80**, 042508 (2009).

[41] V. Barbé, A. Ciamei, B. Pasquiou, L. Reichsöllner, F. Schreck, P. S. Żuchowski, and J. M. Hutson, *Observation of Feshbach resonances between alkali and closed-shell atoms*, Nat. Phys. **14**, 881 (2018).

[42] M. Verma, A. M. Jayich, and A. C. Vutha, *Electron electric dipole moment searches using clock transitions in ultracold molecules*, Phys. Rev. Lett. **125**, 153201 (2020).

[43] J. D. Polet, Y. Chamorro, L. F. Pašteka, S. Hoekstra, M. Tomza, A. Borschevsky, and I. A. Aucar, $\mathcal{P}, \mathcal{T}$*-odd effects in* YbCu, YbAg, *and* YbAu, J. Chem. Phys. **161**, 234302 (2024).

[44] T. Fleig and D. DeMille, *Theoretical aspects of radium-containing molecules amenable to assembly from laser-cooled atoms for new physics searches*, New J. Phys. **23**, 113039 (2021).

[45] I. B. Khriplovich and S. K. Lamoreaux, *General features of EDM experiments*, in *CP Violation Without Strangeness: Electric Dipole Moments of Particles, Atoms, and Molecules* (Springer, Berlin, Heidelberg, 1997) pp. 19–51.

[46] A. Vutha, *A search for the electric dipole moment of the electron using thorium monoxide*, Ph.D. thesis, Yale University, 2011.

[47] J. Baron, W. C. Campbell, D. DeMille, J. M. Doyle, G. Gabrielse, Y. V. Gurevich, P. W. Hess, N. R. Hutzler, E. Kirilov, I. Kozyryev, B. R. O'Leary, C. D. Panda, M. F. Parsons, B. Spaun, A. C. Vutha, A. D. West, and E. P. West (ACME Collaboration), *Methods, analysis, and the treatment of systematic errors for the electron electric dipole moment search in thorium monoxide*, New J. Phys. **19**, 073029 (2017).

[48] J. M. Brown and A. Carrington, *Rotational Spectroscopy of Diatomic Molecules*, Cambridge Molecular Science (Cambridge University Press, Cambridge, England, 2003).

[49] See Supplemental Material at http://link.aps.org/supplemental/10.1103/wlq7-9p41 for detailed information

and complementary results, which includes Refs. [32,40–44,48,50–71].

[50] F. Schreck and K. v. Druten, *Laser cooling for quantum gases*, Nat. Phys. **17**, 1296 (2021).

[51] J. Lee, J. H. Lee, J. Noh, and J. Mun, *Core-shell magneto-optical trap for alkaline-earth-metal-like atoms*, Phys. Rev. A **91**, 053405 (2015).

[52] A. Ciamei, S. Finelli, A. Cosco, M. Inguscio, A. Trenkwalder, and M. Zaccanti, *Double-degenerate Fermi mixtures of* ^{6}Li *and* ^{53}Cr *atoms*, Phys. Rev. A **106**, 053318 (2022).

[53] M. D. Frye, P. S. Żuchowski, and M. Tomza, *Spin–spin interaction and magnetic Feshbach resonances in collisions of high-spin atoms with closed-shell atoms*, Phys. Rev. Res. **6**, 023254 (2024).

[54] M. Tomza, *Prospects for ultracold polar and magnetic chromium–closed-shell-atom molecules*, Phys. Rev. A **88**, 012519 (2013).

[55] H. Ladjimi and M. Tomza, *Diatomic molecules of alkali-metal and alkaline-earth-metal atoms: Interaction potentials, dipole moments, and polarizabilities*, Phys. Rev. A **109**, 052814 (2024).

[56] S. Finelli, A. Ciamei, B. Restivo, M. Schemmer, A. Cosco, M. Inguscio, A. Trenkwalder, K. Zaremba-Kopczyk, M. Gronowski, M. Tomza, and M. Zaccanti, *Ultracold* LiCr*: A new pathway to quantum gases of paramagnetic polar molecules*, PRX Quantum **5**, 020358 (2024).

[57] K. G. Dyall, *Core correlating basis functions for elements 31–118*, Theor. Chem. Acc. **131**, 1 (2012).

[58] Y. J. Franzke, L. Spiske, P. Pollak, and F. Weigend, *Segmented contracted error-consistent basis sets of quadruple-ζ valence quality for one-and two-component relativistic all-electron calculations*, J. Chem. Theory Comput. **16**, 5658 (2020).

[59] A. Sunaga, V. S. Prasannaa, M. Abe, M. Hada, and B. P. Das, *Ultracold mercury–alkali-metal molecules for electron-electric-dipole-moment searches*, Phys. Rev. A **99**, 040501(R) (2019).

[60] C. Baroni, G. Lamporesi, and M. Zaccanti, *Quantum mixtures of ultracold gases of neutral atoms*, Nat. Rev. Phys. **6**, 736 (2024).

[61] H. R. Larsson, H. Zhai, C. J. Umrigar, and G. K.-L. Chan, *The chromium dimer: Closing a chapter of quantum chemistry*, J. Am. Chem. Soc. **144**, 15932 (2022).

[62] E. Tiesinga, J. Kłos, M. Li, A. Petrov, and S. Kotochigova, *Relativistic aspects of orbital and magnetic anisotropies in the chemical bonding and structure of lanthanide molecules*, New J. Phys. **23**, 085007 (2021).

[63] M. L. González-Martínez and P. S. Żuchowski, *Magnetically tunable Feshbach resonances in* Li + Er, Phys. Rev. A **92**, 022708 (2015).

[64] M. B. Kosicki, M. Borkowski, and P. S. Żuchowski, *Quantum chaos in Feshbach resonances of the ErYb system*, New J. Phys. **22**, 023024 (2020).

[65] P. Hamilton, *Preliminary results in the search for the electron electric dipole moment in* PbO*, Ph.D. thesis, Yale University, 2010.

[66] S. Bickman, P. Hamilton, Y. Jiang, and D. DeMille, *Preparation and detection of states with simultaneous spin alignment and selectable molecular orientation in* PbO, Phys. Rev. A **80**, 023418 (2009).

[67] R. F. Curl, *The relationship between electron spin rotation coupling constants and g-tensor components*, Mol. Phys. **9**, 585 (1965).

[68] F. Neese, *Prediction of electron paramagnetic resonance g values using coupled perturbed Hartree–Fock and Kohn–Sham theory*, J. Chem. Phys. **115**, 11080 (2001).

[69] M. Denis, Y. Hao, E. Eliav, N. R. Hutzler, M. K. Nayak, R. G. E. Timmermans, and A. Borschesvky, *Enhanced $\mathcal{P},\mathcal{T}$-violating nuclear magnetic quadrupole moment effects in laser-coolable molecules*, J. Chem. Phys. **152**, 084303 (2020).

[70] T. Fleig and M. K. Nayak, *Electron electric dipole moment and hyperfine interaction constants for* ThO, J. Mol. Spectrosc. **300**, 16 (2014).

[71] D. Wu, C. Zhou, J. J. Bao, L. Gagliardi, and D. G. Truhlar, *Zero-field splitting calculations by multiconfiguration pairdensity functional theory*, J. Chem. Theory Comput. **18**, 2199 (2022).

[72] I. Kopp and J. T. Hougen, *Rotational energy levels of states and intensities in transitions: Applications to some heavier hydrides*, Can. J. Phys. **45**, 2581 (1967).

[73] D. T. Halfen and L. M. Ziurys, *The submillimeter spectrum of* MnH *and* MnD *($X^7\Sigma^+$)*, Astrophys. J. **672**, L77 (2007).

[74] D. T. Halfen and L. M. Ziurys, *Molecules in high spin states III: The millimeter/submillimeter-wave spectrum of the* MnCl *radical ($X^7\Sigma^+$)*, J. Chem. Phys. **122**, 054309 (2005).

[75] C. He, E. Hajiyev, Z. Ren, B. Song, and G.-B. Jo, *Recent progresses of ultracold two-electron atoms*, J. Phys. B **52**, 102001 (2019).

[76] L. Chomaz, I. Ferrier-Barbut, F. Ferlaino, B. Laburthe-Tolra, B. L. Lev, and T. Pfau, *Dipolar physics: A review of experiments with magnetic quantum gases*, Rep. Prog. Phys. **86**, 026401 (2022).

[77] L. Gabardos, S. Lepoutre, O. Gorceix, L. Vernac, and B. Laburthe-Tolra, *Cooling all external degrees of freedom of optically trapped chromium atoms using gray molasses*, Phys. Rev. A **99**, 023607 (2019).

[78] M. Kitagawa, K. Enomoto, K. Kasa, Y. Takahashi, R. Ciuryło, P. Naidon, and P. S. Julienne, *Two-color photoassociation spectroscopy of ytterbium atoms and the precise determinations of s-wave scattering lengths*, Phys. Rev. A **77**, 012719 (2008).

[79] J. Werner, A. Griesmaier, S. Hensler, J. Stuhler, T. Pfau, A. Simoni, and E. Tiesinga, *Observation of Feshbach resonances in an ultracold gas of* ^{52}Cr, Phys. Rev. Lett. **94**, 183201 (2005).

[80] B. Pasquiou, G. Bismut, Q. Beaufils, A. Crubellier, E. Maréchal, P. Pedri, L. Vernac, O. Gorceix, and B. Laburthe-Tolra, *Control of dipolar relaxation in external fields*, Phys. Rev. A **81**, 042716 (2010).

[81] R. Roy, A. Green, R. Bowler, and S. Gupta, *Rapid cooling to quantum degeneracy in dynamically shaped atom traps*, Phys. Rev. A **93**, 043403 (2016).

[82] A. Farolfi, D. Trypogeorgos, G. Colzi, E. Fava, G. Lamporesi, and G. Ferrari, *Design and characterization of a compact magnetic shield for ultracold atomic gas experiments*, Rev. Sci. Instrum. **90**, 115114 (2019).

[83] G. Colzi, E. Fava, M. Barbiero, C. Mordini, G. Lamporesi, and G. Ferrari, *Production of large Bose-Einstein condensates in a magnetic-shield-compatible hybrid trap*, Phys. Rev. A **97**, 053625 (2018).

[84] A. Farolfi, *Spin dynamics in two-component Bose-Einstein condensates*, Ph.D. thesis, University of Trento, 2021.

[85] E. Fava, *Static and dynamics properties of a miscible two-component Bose–Einstein Condensate*, Ph.D. thesis, University of Trento, 2018.

[86] S. Eckel, P. Hamilton, E. Kirilov, H. W. Smith, and D. DeMille, *Search for the electron electric dipole moment using Ω-doublet levels in* PbO, Phys. Rev. A **87**, 052130 (2013).

[87] R. Bause, N. Balasubramanian, T. Fikkers, E. H. Prinsen, K. Steinebach, A. Jadbabaie, N. R. Hutzler, I. A. Aucar, L. c. v. F. Pašteka, A. Borschevsky, and S. Hoekstra, *Prospects for measuring the electron's electric dipole moment with polyatomic molecules in an optical lattice*, Phys. Rev. A **111**, 062815 (2025).

[88] K. Zhu, N. Solmeyer, C. Tang, and D. S. Weiss, *Absolute polarization measurement using a vector light shift*, Phys. Rev. Lett. **111**, 243006 (2013).

[89] N. Vanhaecke and O. Dulieu, *Precision measurements with polar molecules: The role of the black body radiation*, Mol. Phys. **105**, 1723 (2007).

[90] Y. Takahashi, C. Zhang, A. Jadbabaie, and N. R. Hutzler, *Engineering field-insensitive molecular clock transitions for symmetry violation searches*, Phys. Rev. Lett. **131**, 183003 (2023).

[91] N. Hutzler (private communication).

[92] M. Tomza, *Ab initio properties of the ground-state polar and paramagnetic europium–alkali-metal-atom and europium–alkaline-earth-metal-atom molecules*, Phys. Rev. A **90**, 022514 (2014).

[93] A. Ciamei, A. Koza, M. Gronowski, and M. Tomza, *Supporting data for "Ultracold high-spin Σ-state polar molecules for new physics searches"*, 10.5281/zenodo.18467046.

[94] S. Boys and F. Bernardi, *The calculation of small molecular interactions by the differences of separate total energies. some procedures with reduced errors*, Mol. Phys. **19**, 553 (1970).

[95] Y. Wang and M. Dolg, *Pseudopotential study of the ground and excited states of* Yb_2, Theor. Chem. Acc. **100**, 124 (1998).

[96] M. Dolg, U. Wedig, H. Stoll, and H. Preuss, *Energy-adjusted ab initio pseudopotentials for the first row transition elements*, J. Chem. Phys. **86**, 866 (1987).

[97] J. G. Hill, M. Gronowski, and M. Tomza (to be published).

[98] P. J. Knowles, C. Hampel, and H.-J. Werner, *Coupled cluster theory for high spin, open shell reference wave functions*, J. Chem. Phys. **99**, 5219 (1993).

[99] H.-J. Werner, P. J. Knowles, G. Knizia, F. R. Manby, and M. Schütz, *Molpro: A general-purpose quantum chemistry program package*, WIREs Comput. Mol. Sci. **2**, 242 (2012).

[100] H.-J. Werner, P. J. Knowles, G. Knizia, F. R. Manby, M. Schütz *et al.*, *Molpro, version 2022, a package of ab initio programs*, see https://www. molpro.net.

[101] M. Kállay, P. R. Nagy, D. Mester, Z. Rolik, G. Samu, J. Csontos, J. Csóka, P. B. Szabó, L. Gyevi-Nagy, B. Hégely, I. Ladjánszki, L. Szegedy, B. Ladóczki, K. Petrov, M. Farkas, P. D. Mezei, and A. Ganyecz, *Mrcc, a quantum chemical program*, see https://www.mrcc.hu.

[102] J. F. Stanton and R. J. Bartlett, *The equation of motion coupled-cluster method. A systematic biorthogonal approach to molecular excitation energies, transition probabilities, and excited state properties*, J. Chem. Phys. **98**, 7029 (1993).

[103] H. Werner and P. J. Knowles, *An efficient internally contracted multiconfiguration–reference configuration interaction method*, J. Chem. Phys. **89**, 5803 (1988).

[104] D. A. Matthews, L. Cheng, M. E. Harding, F. Lipparini, S. Stopkowicz, T.-C. Jagau, P. G. Szalay, J. Gauss, and J. F. Stanton, *Coupled-cluster techniques for computational chemistry: The CFOUR program package*, J. Chem. Phys. **152**, 214108 (2020).

[105] J. F. Stanton, J. Gauss, L. Cheng, M. E. Harding, D. A. Matthews, and P. G. Szalay, *CFOUR, Coupled-Cluster techniques for Computational Chemistry, a quantum-chemical program package*, With contributions from A. Asthana, A. A. Auer, R. J. Bartlett, U. Benedikt, C. Berger, D. E. Bernholdt, S. Blaschke, Y. J. Bomble, S. Burger, O. Christiansen *et al.*, and the integral packages MOLECULE (J. Almlöf and P. R. Taylor), PROPS (P. R. Taylor), ABACUS (T. Helgaker, H. J. Aa. Jensen, P. Jørgensen, and J. Olsen), and ECP routines by A. V. Mitin and C. van Wüllen. For the current version, see http://www.cfour.de.

[106] T. Saue *et al.*, *The Dirac code for relativistic molecular calculations*, J. Chem. Phys. **152**, 204104 (2020).

[107] S. Knecht, H. J. A. Jensen, and T. Fleig, *Large-scale parallel configuration interaction. II. Two- and four-component double-group general active space implementation with application to* BiH, J. Chem. Phys. **132**, 014108 (2010).

[108] E. Lindroth, B. Lynn, and P. Sandars, *Order α^2 theory of the atomic electric dipole moment due to an electric dipole moment on the electron*, J. Phys. B **22**, 559 (1989).

[109] M. Kozlov, *Semiempirical calculations of P- and P, T-odd effects in diatomic molecules-radicals*, Zh. Eksp. Teor. Fiz. **89**, 1933 (1985).

[110] V. Flambaum, *Spin hedgehog and collective magnetic quadrupole moments induced by parity and time invariance violating interaction*, Phys. Lett. B **320**, 211 (1994).

[111] L. V. Skripnikov, A. V. Titov, and V. V. Flambaum, *Enhanced effect of $\mathcal{CP}$-violating nuclear magnetic quadrupole moment in a* HfF^+ *molecule*, Phys. Rev. A **95**, 022512 (2017).

[112] D. Peng, N. Middendorf, F. Weigend, and M. Reiher, *An efficient implementation of two-component relativistic exact-decoupling methods for large molecules*, J. Chem. Phys. **138**, 184105 (2013).

[113] F. Neese, *The ORCA program system*, WIREs Comput. Mol. Sci. **2**, 73 (2012).

[114] F. Neese, *Software update: The ORCA program system—version 6.0*, Comput. Mol. Sci. **15**, e70019 (2025).